Hindawi
Shock and Vibration
Volume 2024, Article ID 9753919, 1 page
https://doi.org/10.1155/2024/9753919

Retraction

Retracted: High-Resolution Direction of Arrival Estimation of Underwater Multitargets Using Swarming Intelligence of Flower Pollination Heuristics

Shock and Vibration

Received 23 January 2024; Accepted 23 January 2024; Published 24 January 2024

This article has been retracted by Hindawi following an investigation undertaken by the publisher [1]. This investigation has uncovered evidence of one or more of the following indicators of systematic manipulation of the publication process:

(1) Discrepancies in scope

(2) Discrepancies in the description of the research reported

(3) Discrepancies between the availability of data and the research described

(4) Inappropriate citations

(5) Incoherent, meaningless and/or irrelevant content included in the article

(6) Manipulated or compromised peer review

The presence of these indicators undermines our confidence in the integrity of the article's content and we cannot, therefore, vouch for its reliability. Please note that this notice is intended solely to alert readers that the content of this article is unreliable. We have not investigated whether authors were aware of or involved in the systematic manipulation of the publication process.

Wiley and Hindawi regrets that the usual quality checks did not identify these issues before publication and have since put additional measures in place to safeguard research integrity.

We wish to credit our own Research Integrity and Research Publishing teams and anonymous and named external researchers and research integrity experts for contributing to this investigation.

The corresponding author, as the representative of all authors, has been given the opportunity to register their agreement or disagreement to this retraction. We have kept a record of any response received.

References

[1] N. Ahmed, H. Wang, S. Tu et al., "High-Resolution Direction of Arrival Estimation of Underwater Multitargets Using Swarming Intelligence of Flower Pollination Heuristics," *Shock and Vibration*, vol. 2022, Article ID 5876874, 16 pages, 2022.

Hindawi
Shock and Vibration
Volume 2022, Article ID 5876874, 16 pages
https://doi.org/10.1155/2022/5876874

Research Article

High-Resolution Direction of Arrival Estimation of Underwater Multitargets Using Swarming Intelligence of Flower Pollination Heuristics

Nauman Ahmed,[1] **Huigang Wang**,[1] **Shanshan Tu**,[2] **Norah A.M. Alsaif**,[3] **Muhammad Asif Zahoor Raja**,[4] **Muhammad Kashif**,[5] **Ammar Armghan**,[6] **Yasser S. Abdalla**,[7,8] **Wasiq Ali**,[5] **and Farman Ali**[8,9]

[1]*School of Marine Science and Technology Northwestern Polytechnical University, Xian, Shaanxi, China*
[2]*Engineering Research Center of Intelligent Perception and Autonomous Control, Faculty of Information Technology, Beijing University of Technology, Beijing 100124, China*
[3]*Department of Physics, College of Science, Princess Nourah bint Abdulrahman University, P. O. Box 84428, Riyadh 11671, Saudi Arabia*
[4]*Future Technology Research Center, National Yunlin University of Science and Technology, 123 University Road, Section 3, Douliou, Yunlin 64002, Taiwan*
[5]*Department of Electrical and Computer Engineering, COMSATS University Islamabad Attock Campus, Islamabad, Pakistan*
[6]*Department of Electrical Engineering, College of Engineering, Jouf University, Sakaka 72388, Saudi Arabia*
[7]*Department of Computer Engineering and Networks, College of Computer and Information Sciences, Jouf University, Sakakah, Saudi Arabia*
[8]*Faculty of Technology and Education, Suez University, Suez, Egypt*
[9]*Department of Electrical Engineering, Qurtuba University of Science and IT, Dera Ismail Khan 29050, Pakistan*

Correspondence should be addressed to Nauman Ahmed; nauman@mail.nwpu.edu.cn, Shanshan Tu; sstu@bjut.edu.cn, and Farman Ali; drfarmanali.optics@qurtuba.edu.pk

Received 6 January 2022; Revised 19 April 2022; Accepted 21 April 2022; Published 30 June 2022

Academic Editor: Yuxing Li

Developing the parameter estimation, particularly direction of arrival (DOA), utilizing the swarming intelligence-based flower pollination algorithm (FPA) is considered an optimistic solution. Therefore, in this paper, the features of FPA are applied for viable DOA in the case of several robust underwater scenarios. Moreover, acoustic waves impinging from the far-field multitarget are evaluated using the different number of hydrophones of uniform linear array (ULA). The measuring parameters like robustness against noise and element quantity, estimation accuracy, computation complexity, various numbers of hydrophones, variability analysis, frequency distribution and cumulative distribution function of root mean square error (RMSE), and resolution ability are applied for analyzing the performance of the proposed model with additive white Gaussian noise (AWGN). For this purpose, particle swarm optimization (PSO), minimum variance distortion-less response (MVDR), multiple signal classification (MUSIC), and estimation of signal parameter via rotational invariance technique (ESPRIT) standard counterparts are employed along with Crammer–Rao bound (CRB) to improve the worth of the proposed setup further. The proposed scheme for estimating the DOA generates efficient outcomes compared to the state-of-the-art algorithms over the Monte Carlo simulations.

1. Introduction

Swarming intelligence of evolutionary algorithms is a significant development in signal processing for direction of arrival (DOA) estimation of underwater multitargets [1, 2]. For solving such problems, subspace-based methods were used like multiple signal classification (MUSIC) [3]. If used in a constraint environment like assuming incoherent

sources, with a specified number of snapshots and high SNR signals, these methods give good results. But due to these limitations, it can only be applied to very few scenarios and problems. Parametric methods like maximum likelihood (ML) [4, 5] are also used to address such issues, but they are computationally complex, which impedes the fertility of application. Previously, most of the published research validated the performance of DOA estimators using asymptotic assumptions, which requires either a high signal-to-noise ratio or a more significant number of samples, which are not specific in many real-life problems [6, 7]. DOA estimator accuracy is dependent on the signal power and the rate of transmission, which are beyond the control of the system designer [8]. Therefore, such systems operate in a low SNR, estimating accurate angular localization, a challenging task [9]. New intelligent optimization algorithms have been proposed recently for estimation of DOA like genetic algorithm (GA) [9], differential evolution (DE) method [8], particle swarm optimization (PSO), seeker optimization algorithm (SOA), sine cosine algorithm (SCA), invasive weed optimization (IWO) [10], and squirrel search algorithm (SSA) [11]. In [12], GA is proposed with accurate and reliable results for the estimation of the parameters of DOA problems, and the performances of the GA, ML, and MUSIC algorithm have been compared with different variants of SNR, computational cost, and the number of snapshots. The detection probability is modeled in [13], through the active sonar equation for probability hypothesis density (PHD) and cardinalized PHD (CPHD). Novel complexity measure is proposed in [14] for improving permutation entropy (PE) and analyzing the time series. Similarly, missing amplitude information and single scale problem in PE are addressed in [15] through refined composite multiscale reverse weighted PE (RCMRWE). A modified version of the GA is applied to the nonlinear and highly nonlinear function to estimate the parameters of DOA as presented in [16]. In [17, 18], PSO algorithm and pattern search algorithm were developed to estimate the parameters of the multimodal function. In [19], the PSO ML estimator shows very healthy and reliable results as compared to conventional parameter estimation techniques for DOA. Using the ant colony optimization (ACO) by extending the pheromone, DOA parameters are estimated in [20], with outstanding results and low computational complexity. In [21], the artificial bee colony (ABC) algorithm is used to achieve higher statistical performance. A high degree of freedom for DOA is studied in [22] using Cuckoo search algorithm. The analytical model was discussed for the proposed approach in terms of fitness function, SNR, and cumulative distributive function. In [23], the authors have proposed adaptive FPA mechanism in order to localize the nodes in wireless sensor networks. Back in 2019, a Squirrel Search Algorithm (SSA) was proposed, which is a novel numerical optimization algorithm. It focuses on the foraging and gliding behavior of flying squirrels to determine their efficient way of locomotion. Gliding is a powerful technique used by small mammals for traveling long distances. The present work mathematically models this behavior to realize the process of optimization. These features may be helpful to improve convergence and reduce the number of iterations of the SSA algorithm to determine the ML DOA estimate [24].

In this study, optimization strength of nature-inspired heuristics of flower pollination algorithm (FPA) is exploited for possible DOA estimation in case of different scenarios of the underwater environment using a uniform linear array (ULA) of hydrophones for influencing acoustic waves from far-field multitargets. The high resolution for close space targets is achieved using fewer snapshots viably with FPA by investigating the global minima of the highly nonlinear cost function of ULA with multiple local minima. Performance analysis is conducted for different number of targets employing estimation accuracy, robustness against noise, and number of hydrophones in the presence of additive white Gaussian measurement noise, and comparative studies with MVDR, MUSIC, Root MUSIC, and ESPRIT counterparts along with Crammer–Rao bound analysis reveals the worth of the scheme for estimating DOA parameters, which are further endorsed from the results of Monte Carlo simulations.

The rest of the paper is arranged as follows: Section 2 defines the mathematical model for ULA. The conventional beamforming (CBF) algorithm, MVDR, MUSIC, Root MUSIC, and ESPRIT are explained with their procedure for the DOA problem in Section 3. Performance analysis of algorithms concerning RMSE is illustrated in Section 4. Finally, Section 5 explains the main contributions of the proposed study.

2. Mathematical Model

In this study, the ULA of hydrophones is used for 1D-DOA estimation. So, according to the characteristics of ULA, the impinged plane waves from the far-field region are phase-shifted versions of consecutive hydrophones as explained in Figure 1. The angle of arrival [25, 26] can be denoted as

$$\theta = [\theta_1, \theta_2, \theta_3, \ldots, \theta_D]. \tag{1}$$

Here, θ_D is the associated angle to the D^{th} acoustic source.

$$\begin{aligned} \mathbf{z}(t) &= [z_1(t), z_2(t), \ldots, z_W(t)], \\ \mathbf{g}(\theta_i) &= \left[1, e^{(-jkd\sin(\theta_i))}, e^{(-jk2d\sin(\theta_i))}, \ldots, e^{-jk(W-1)d\sin(\theta_i)}\right]^T, \\ \mathbf{G}(\theta) &= [\mathbf{g}(\theta_1), \mathbf{g}(\theta_2), \ldots, \mathbf{g}(\theta_D)]. \end{aligned} \tag{2}$$

Here, $k = 2\pi/\lambda$, while λ is the wave length. $\mathbf{z}(\mathbf{t})$ is the hydrophone's output vector with dimension $W \times 1$ and can be known as array response.

$$\mathbf{z}(\mathbf{t}) = \mathbf{G}(\theta)\mathbf{y}(t) + \mathbf{v}(t). \tag{3}$$

The steering matrix G of dimension $W \times D$ comprises the time delay entities of signals for each hydrophone. Here, $\mathbf{v}(\mathbf{t})$ is additive white Gaussian noise of zero mean with a dimension of $W \times 1$. The covariance matrix [27, 28] is defined as

$$\mathbf{R} = E\left[\mathbf{z}(t)\mathbf{z}^H(t)\right]. \tag{4}$$

The previous equation can be written when a finite number of snapshots are available:

$$\mathbf{R} = \frac{1}{K}\sum_{n=1}^{K}\mathbf{z}(n)\mathbf{z}^H(n), \tag{5}$$

where $E[.]$ and $[.]^H$ are ensemble average and Hermitian operators, respectively. So the correlation matrix [29, 30] can be written as

$$\mathbf{R} = \mathbf{G}\mathbf{R}_s\mathbf{G}^H + \sigma^2\mathbf{I}_D. \tag{6}$$

where $\mathbf{R}_y$ is the correlation associated with signal and $\sigma^2\mathbf{I}_D$ is the noise correlation matrix.

3. DOA Estimation

Generally, DOA estimation algorithms are divided into two categories, i.e., CBF techniques and subspace-based techniques. In this work, the performance analysis has been taken for both the CBF and subspace-based algorithms under varying noise levels for different acoustic sources.

3.1. Particle Swarm Optimization. The heuristics of PSO was proposed by Kennedy and Eberhart having motivation from the pool of birds congregating for food in a random manner [31]. The idea of seeking food is a heuristic approach because all the birds have the information of distance but are not familiar with the explicit location of food. They seek the food by exchanging their search information via crossover and kid production method. The PSO is introduced for the pool of applications almost in every walk of engineering [32, 33]. In this work, PSO performs searching via a swarm of particles that updates recursively. To approach the optimal solution, each particle (DOAs) moves in the direction to its previously best ($p$best) position and the global best ($g$best) position in the swarm.

$$\begin{aligned}\mathbf{v}_i(n+1) = {} & \boldsymbol{\omega}\mathbf{v}_\mathbf{i}(\mathbf{n}) + \mathbf{c}_1\mathbf{r}_1\left(\boldsymbol{\theta}_\mathbf{i}(\mathbf{n}) - \boldsymbol{\theta}_\mathbf{pbest}\right) \\ & + \mathbf{c}_2\mathbf{r}_2\left(\boldsymbol{\theta}_\mathbf{i}(\mathbf{n}) - \boldsymbol{\theta}_\mathbf{gbest}\right).\end{aligned} \tag{7}$$

$$\boldsymbol{\theta}_i(n+1) = \boldsymbol{\theta}_i(n) + \mathbf{v}_i(n+1). \tag{8}$$

Here, $\theta_{p\text{best}}$ and $\theta_{g\text{best}}$ can be calculated as

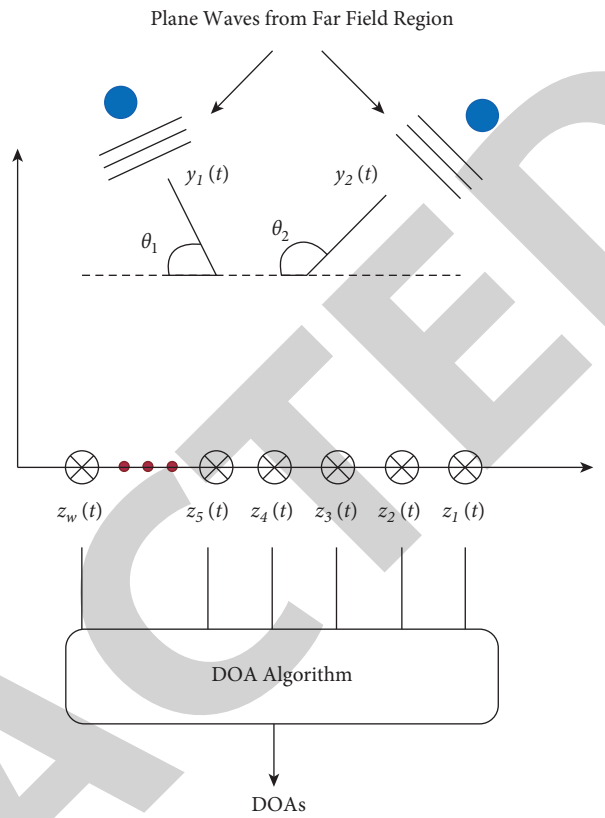

Figure 1: DOA estimation model.

$$\begin{aligned}\boldsymbol{\theta}_{p\text{best}}(i) &= \text{argmin}_{i=1,\ldots,K} f\left(\theta_n(i)\right), \\ \boldsymbol{\theta}_{g\text{best}}(i) &= \text{argmin}_{n=1,\ldots,N} f\left(\theta_n(i)\right).\end{aligned} \tag{9}$$

Here, i denotes the particle index, n is the current iteration number, and $f(\theta_n(i))$ is the fitness function that can be defined as

$$f(\theta_e) = \left|\mathbf{z}\boldsymbol{\theta}_\mathbf{e}(\mathbf{t}) - \mathbf{z}\boldsymbol{\theta}_\mathbf{a}(\mathbf{t})\right|^2. \tag{10}$$

And, the parameters ω, c_1, c_2, r_1, and r_2 are inertia weight, two positive constants, and two random parameters within [0, 1], respectively. The velocity v and positions (DOAs) of particles are updated with equations (9) and (10).

3.2. Basis Principle of FPA. The features of pollination scheme, flower reliability, and behavior of the pollinator can be analyzed efficiently by the following principles:

(1) The global pollination scheme consists of cross-pollination and biotic methods, while pollinators perform levy flights with pollen (global optimization)

(2) The local pollination mechanism consists of self-pollination and abiotic methods (local optimization) [34]

(3) A switch probability $p \epsilon [0, 1]$ is designed to control global pollination and local pollination schemes

Figure 2: Flow chart of FPA.

In the complete pollination process, the local pollination scheme can experience a large quantity of fraction p. Its reason can be environmental factors like wind and physical proximity. Generally, many flowers can grow on a plant, and pollen gametes from each flower can be released in billions. However, here we suppose that every plant has the ability to harvest only one flower and only one pollen gamete can be produced from each flower. Therefore, plant, flower, and pollen gamete are easy to identify for finding the solution to a problem. The above assumption develops the most straightforward way that solution can be equal to a pollen gamete and a flower. In future research, especially for multiobjective optimization problems, different numbers of flowers can be associated with each plant and multiple pollen gametes can be assigned to each flower. A flower-based algorithm, known as flower pollination algorithm (FPA), can

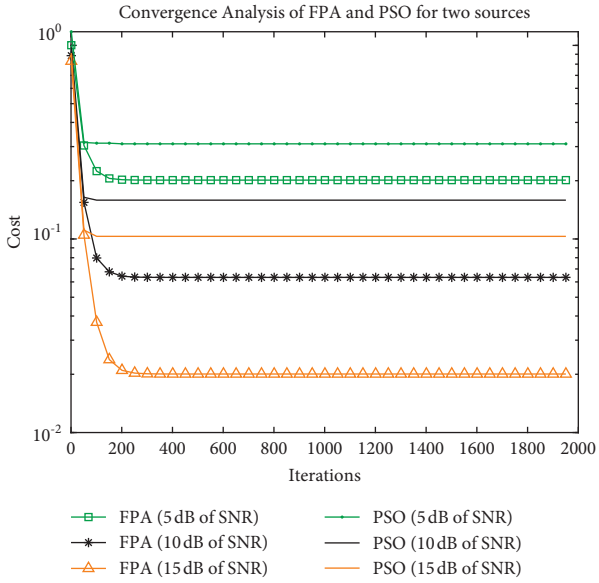

Figure 3: Convergence analysis of FPA for two sources.

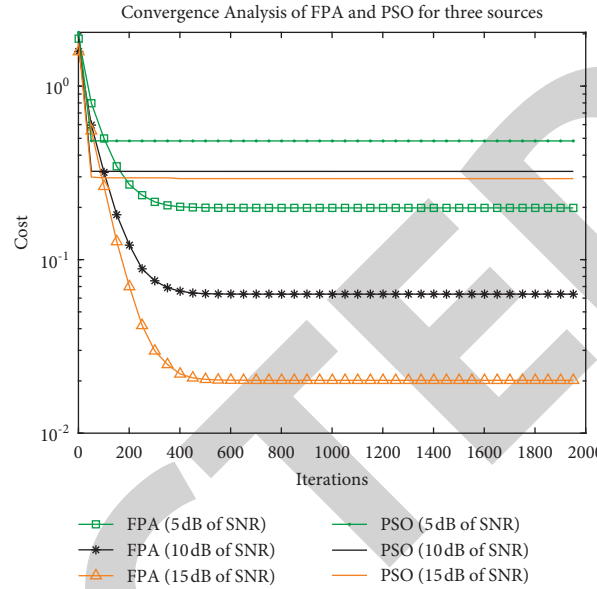

Figure 4: Convergence analysis of FPA for three sources.

be designed from the above principles and arguments. Global pollination and local pollination are two major stages of this algorithm [35]. In the phase of global pollination, insects work as pollinators for carrying flower pollens over long distances because of their capability to move and fly for a more extended range. In this way, fittest reproduction and pollination can be ensured. Flower reliability phenomena and the first rule of global pollination step can be mathematically [36, 37] described as

$$\theta_i(n+1) = \theta_i(n) + L\left(\theta_i(n) - \theta_{\text{best}}\right). \tag{11}$$

Here, pollen i is represented by $\theta_i(n)$ at iteration n, while at current iteration, the best value among all values is denoted by θ_{best}. Pollination strength is shown with parameter L, which represents step size. Levy flight mechanism can be used accurately to analyze the property of insects to travel over long distances using many steps. Thus, from Levy distribution, we develop $L > 0$. In the end, the best result can be referred to as the best approximated angle.

$$L = \lambda\Gamma(\lambda)\sin\left(\frac{\pi\lambda}{2}\right)\left(\pi.s^{(1+\lambda)}\right)^{-1}. \tag{12}$$

The standard gamma function is represented by $\Gamma(\lambda)$ with $\lambda = 1.5$, and s consists of Gaussian distributions U and V described as

$$s = U.|V|^{-1/\lambda}, \tag{13}$$

where $U \sim N(0, \sigma^2)$ and $V \sim N(0, 1)$, and σ^2 can be computed as

$$\sigma^2 = \left\{\frac{\Gamma(1+\lambda)}{\lambda\Gamma[(1+\lambda)/2]}.\frac{\sin(\pi\lambda/2)}{2^{(\lambda-1)/2}}\right\}^{1/\lambda}. \tag{14}$$

Local pollination step and flower reliability phenomena can be written as

$$\theta_i(n+1) = \theta_i(n) + \varepsilon\left(\theta_j(n) - \theta_k(n)\right). \tag{15}$$

Two arbitrary pollens produced from unlike flowers of the similar plant are denoted with $\theta_j(n)$ and $\theta_k(n)$ in the above mathematical model. This behavior shows the reliability of a flower in a limited community. Mathematically, these solutions are selected from the same population with a random walk of ϵ drawn from a uniform distribution in [0, 1]. Many of the flower pollination processes happen at both global and local levels. Practically local flower pollens pollinate the nearby flowers and flower patches or those not so from them. Thus, using this property, a switch or proximity probability p_s (Rule 3) is developed to shift among global mutual pollination and complete local pollination. By applying switch probability, $p_s = 0.5$ can be used as starting value, and after this, a suitable range of parameters can be developed. The literature shows that $p_s = 0.8$ is appropriate for many practical applications.

3.3. DOA Estimation Using FPA. The general goal of DOA estimation is a continuous optimization that is used to find the θ_{best} which satisfies

$$f\left(\theta_{\text{best}}\right) = \min_{\theta \epsilon S} f(\theta), \tag{16}$$

where $S \epsilon R^D$ and $f(\theta)$ comprise the cost values of the corresponding solution θ. The cost function of DOA estimation can be defined as

$$f(\theta) = \left|z_e(\theta) - z\left(\theta_a\right)\right|^2, \tag{17}$$

where $z_e(\theta)$ is the estimated (approximated using optimized parameters) array output and $z(\theta_a)$ is the actual array out. Therefore, the actual goal of the optimizer is to compute the associated argument for the minimum cost of the cost function as shown in Figure 2. Hence, the population of N individuals will be used to solve the optimization problem

Table 1: Estimation accuracy for two sources.

SNR = 5 dB, snapshots = 20, hydrophones = 8, $d = \lambda/2$							
Algorithms		FPA	ESPRIT	RMUSIC	MUSIC	MVDR	PSO
$\theta_1 = 30$	Mean	30.005	29.680	26.125	31.980	32.036	33.549
	Variance	0.0162	5.490	347.70	1.932	0.869	33.549
$\theta_1 = 35$	Mean	34.953	35.693	35.246	32.993	33.036	278.68
	Variance	0.008	12.373	33.661	1.960	0.869	476.42

Table 2: Estimation accuracy for three sources.

SNR = 5 dB, snapshots = 20, hydrophones = 8, $d = \lambda/2$							
Algorithms		FPA	ESPRIT	RMUSIC	MUSIC	MVDR	PSO
$\theta_1 = 30$	Mean	29.999	29.099	11.961	38.710	39.666	37.447
	Variance	0.0188	46.4054	854.4187	55.3792	46.2022	439.3751
$\theta_2 = 40$	Mean	39.998	39.792	38.310	41.033	41.153	47.041
	Variance	0.0205	14.4508	47.6986	53.7322	44.8432	345.3394
$\theta_1 = 50$	Mean	50.007	50.686	48.330	42.483	42.920	51.160
	Variance	0.0295	14.3758	19.3924	51.7431	40.6736	138.6291

Table 3: Estimation accuracy for four sources.

SNR = 5 dB, snapshots = 20, sydrophones = 8, $d = \lambda/2$							
Algorithms		FPA	ESPRIT	RMUSIC	MUSIC	MVDR	PSO
$\theta_1 = 10$	Mean	10.798	6.754	−23.206	21.393	23.207	9.859
	Variance	63.4	137.7	753.8	98.5	97.0	1224.0
$\theta_2 = 20$	Mean	20.248	18.989	14.247	24.713	25.583	41.079
	Variance	16.3	18.9	58.3	102.3	94.3	1032.8
$\theta_3 = 30$	Mean	30.001	30.628	25.541	28.473	27.853	39.7725
	Variance	0.0204	21.7581	69.7347	93.6560	89.8585	550.2132
$\theta_4 = 40$	Mean	39.995	41.852	37.238	31.137	29.893	47.3674
	Variance	0.0274	29.1674	35.1613	75.3313	78.6620	391.5863

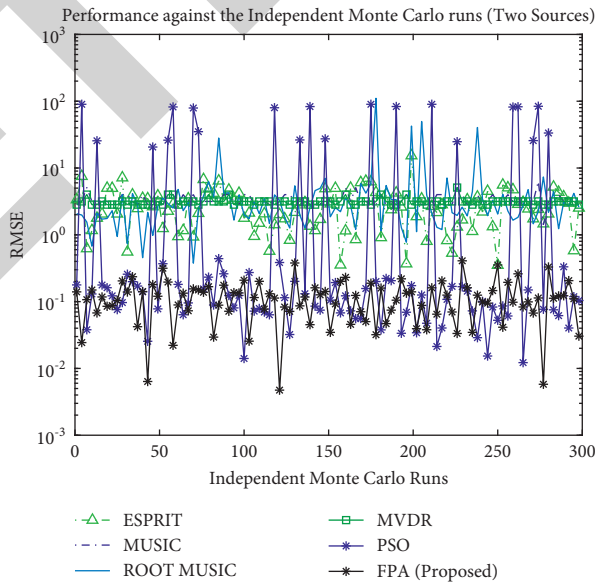

Figure 5: Performance against independent Monte Carlo runs for two sources with 5 dB of SNR.

having T iterations (trials). The set of D-dimensional vectors (total N vectors) for i iteration can be denoted as

$$\theta_1(i), \theta_2(i), \theta_3(i), \ldots, \theta_N(i). \quad (18)$$

Hence, the best solution at iteration i can be found as

$$\theta_{\text{best}}(i) = \text{argmin}_{n=1,\ldots,N} f(\theta_n(i)). \quad (19)$$

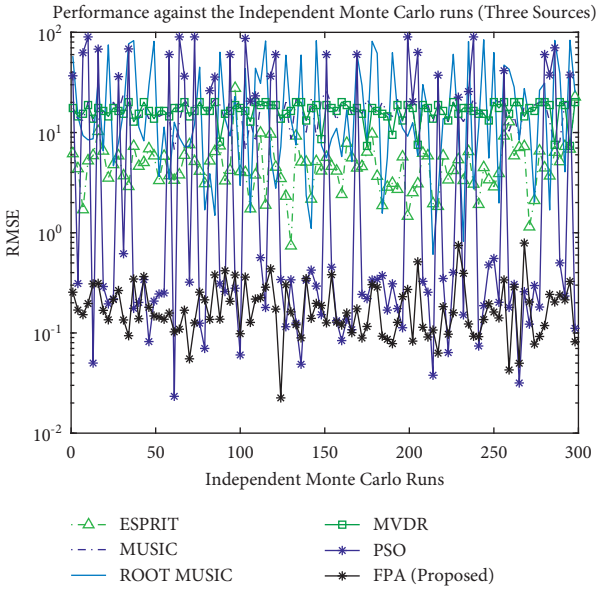

Figure 6: Performance against independent Monte Carlo runs for three sources with 5 dB of SNR.

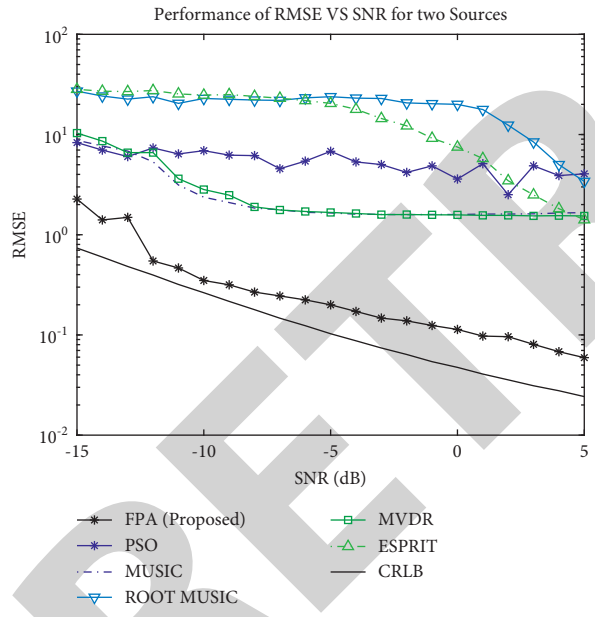

Figure 7: Performance of RMSE vs SNR for two sources.

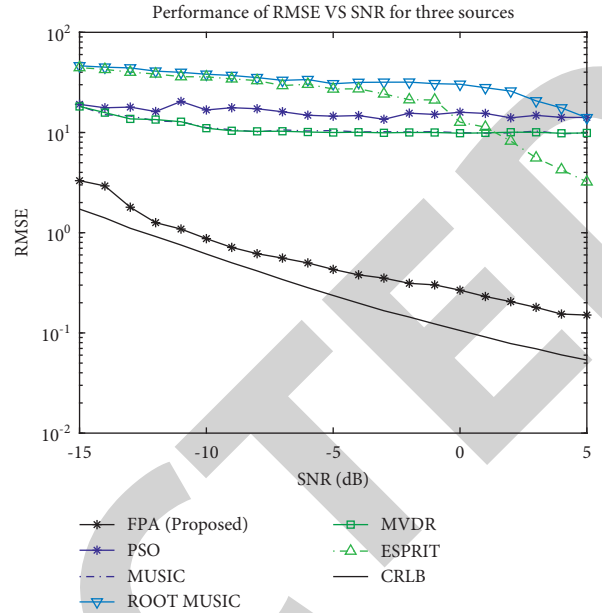

Figure 8: Performance of RMSE vs SNR for three sources.

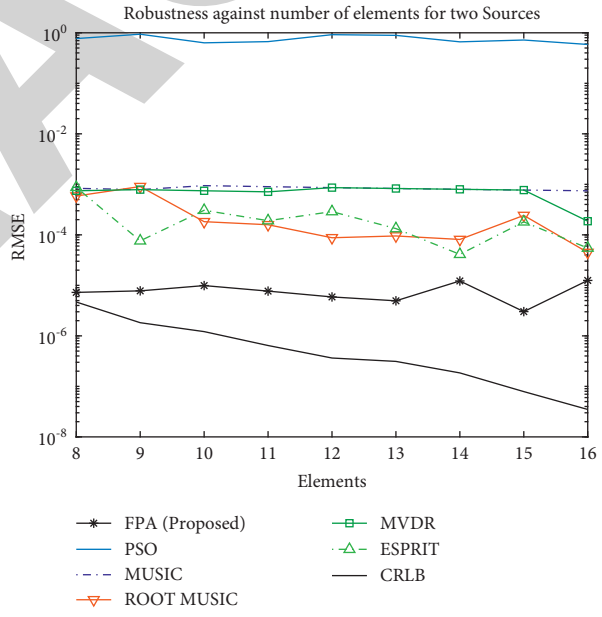

Figure 9: Robustness against the number of elements for two sources of 5 dB of SNR.

4. Experimental Results and Comparison

In this section, numerous simulations have been carried out to analyze the performance of the FPA against the state-of-the-art algorithms. The performance has been studied in terms of estimation accuracy, convergence analysis, robustness against noise, and the robustness against the number of hydrophones used in the array. The conditions for FPAs are also depicted in this section. The measures of performance illustrate the comprehensive analysis of FPAs as explained in the following areas.

4.1. Convergence Analysis. In this section, we examined the performance of FPA and PSO in terms of convergence. The performance is analyzed for two and three sources with the varying noise level. Figures 3 and 4 show that the FPA converged towards the minimum cost as compared to that of PSO.

4.2. Estimation Accuracy. The estimation accuracy of MVDR, MUSIC, Root MUSIC, ESPRIT, PSO, and FPA is examined here by taking signal sources with different positions and different noise levels. The noise is assumed to be

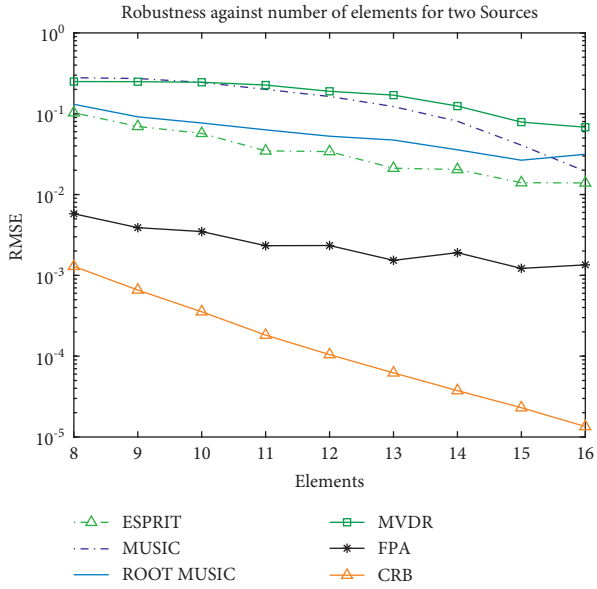

Figure 10: Robustness against the number of elements for two sources of 10 dB of SNR.

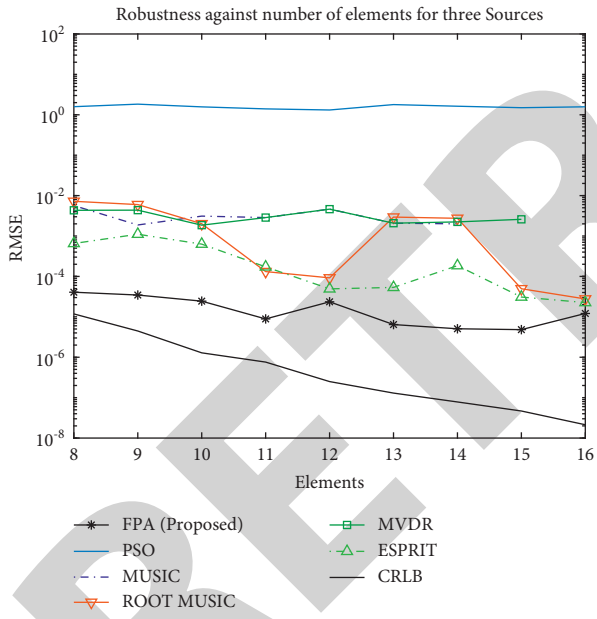

Figure 11: Robustness against the number of elements for three sources of 5 dB of SNR.

additive white Gaussian with zero means. The statistical measures of the mean and variance have been calculated from 300 independent Monte Carlo simulations as discussed in the tables for each algorithm. It can be seen from Tables 1–3 that the best performance is for FPAs in all different noise levels and in all two cases of Monte Carlo simulations (mean, variance).

4.3. Performance against the Independent Monte Carlo Runs. The performance metrics are analyzed by calculating RMSE that is defined as follows:

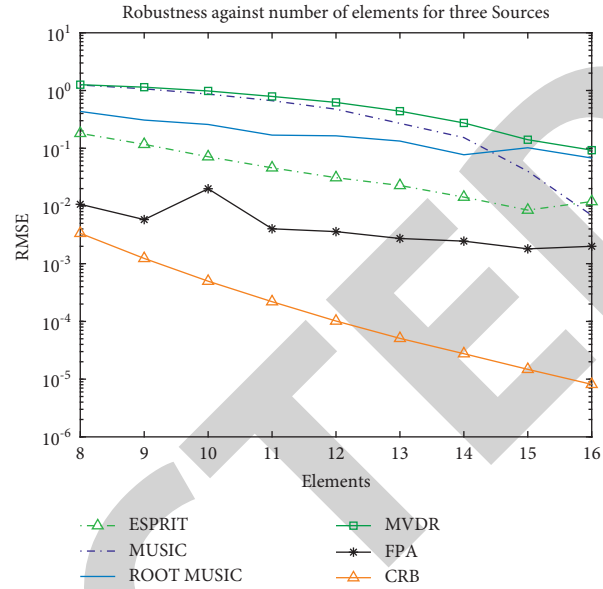

Figure 12: Robustness against the number of elements for three sources of 10 dB of SNR.

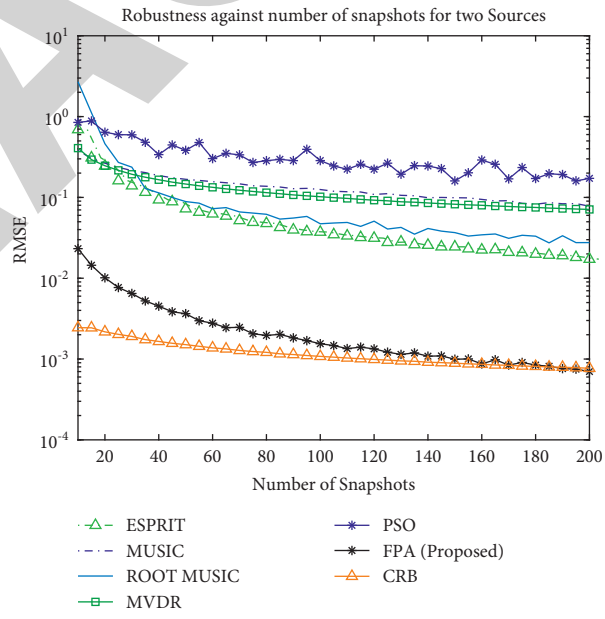

Figure 13: Robustness against snapshots for two sources.

$$\text{RMSE} = \sqrt{\sum_{K}\sum_{i=1}^{D}\frac{1}{\text{KD}}\left(\theta_{i(a)} - \theta_{i(e)}\right)^2}. \tag{20}$$

Here, $\theta_{i(a)}$ is the actual DOA and $\theta_{i(e)}$ is the estimated DOA.

In this section, the performance has been analyzed against the independent Monte Carlo runs. The simulation results show that the oscillations of the maximum and minimum of RMSE describe the best and worst performance of the algorithm. Hence, the reliability of the FPA outperforms that of the MVDR, MUSIC, RMUSIC, and ESPRIT and PSO algorithm for independent Monte Carlo runs as shown in Figures 5 and 6.

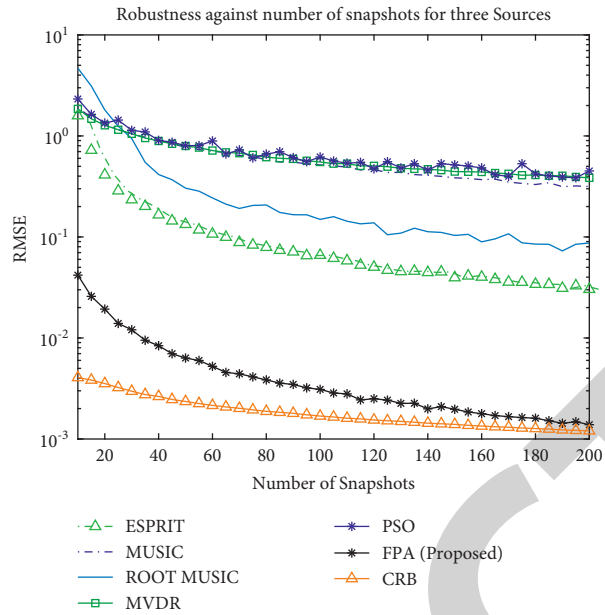

Figure 14: Robustness against snapshots for three sources.

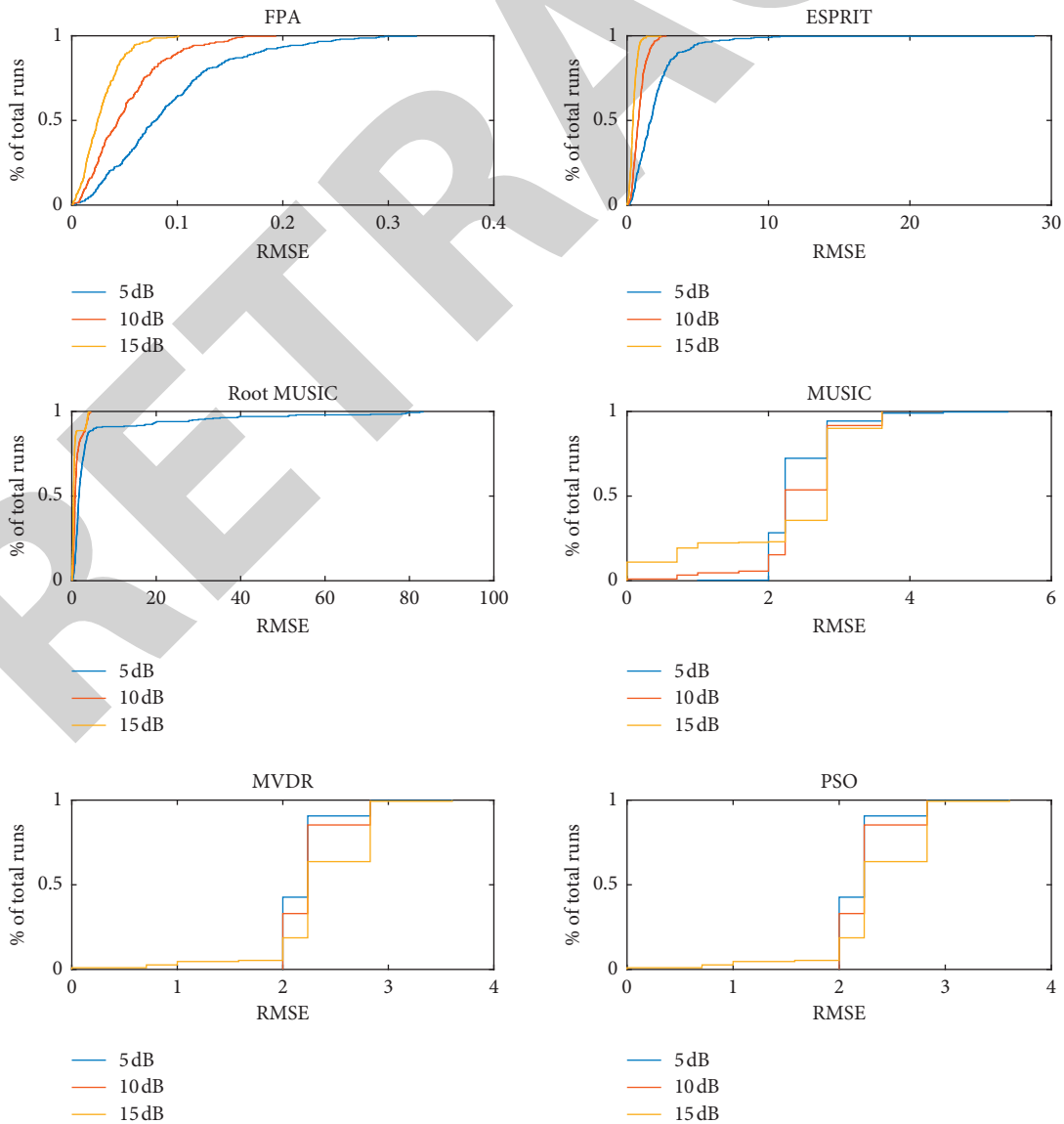

Figure 15: CDF of RMSE for two sources.

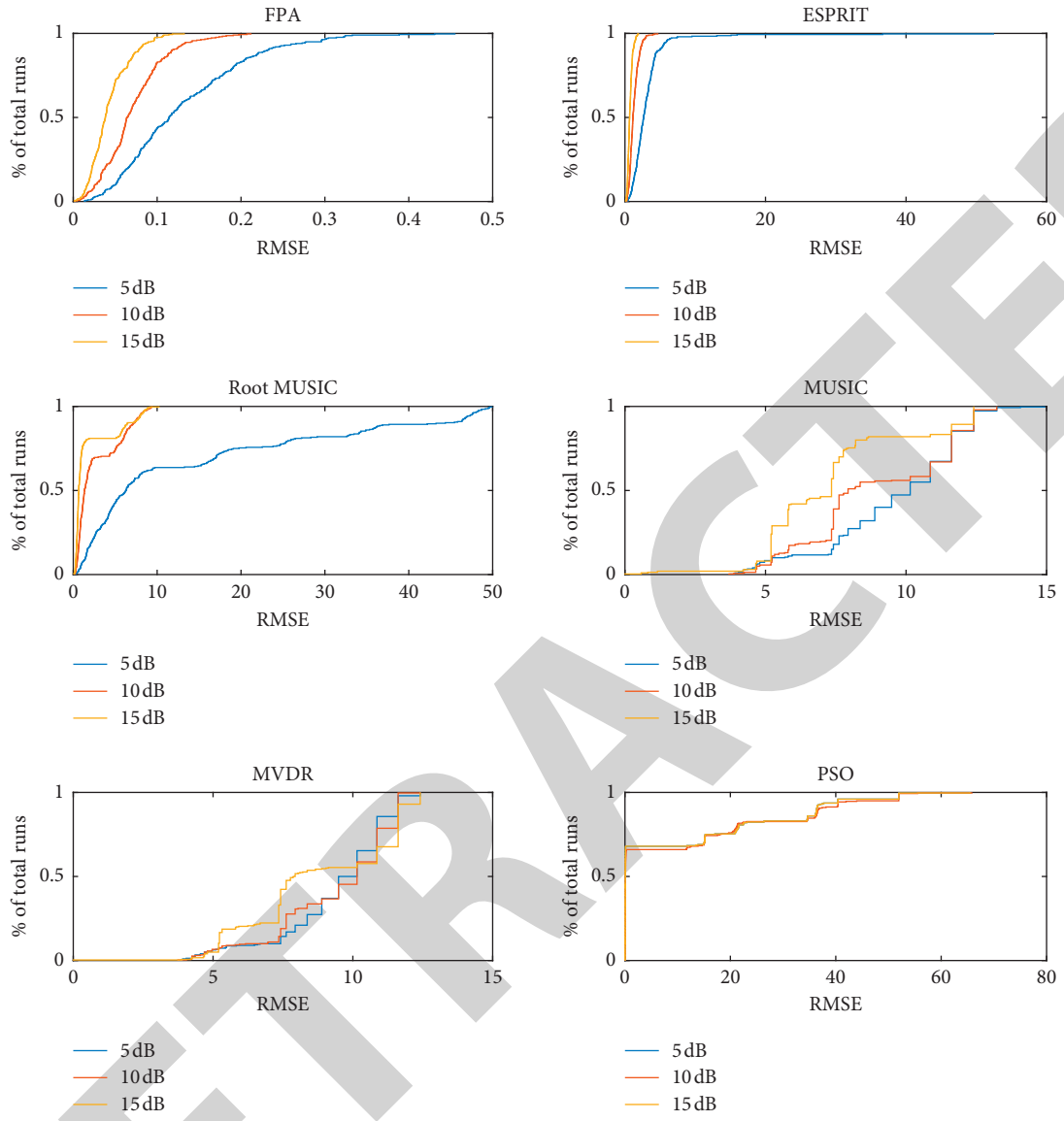

Figure 16: CDF of RMSE for three sources.

4.4. Robustness against Noise. In this section, the performance of these algorithms is measured by calculating the RMSE under varying levels of additive white noise. The convergence of RMSE also depicts performance analysis of such algorithms with the different number of signal sources having different DOAs.

We have used eight hydrophones, and the number of snapshots is 20 for two sources located at 30° and 35° and for three sources situated at 30°, 34°, and 50°. The result analysis in Figures 7 and 8 presents that the RMSE is a function of SNR. As the SNR increases, the RMSE decreases substantially. It can be seen that the FPA is robust enough to produce excellent results even in the presence of low SNR as compared to the other algorithms. CRB has also validated the performances of the algorithms.

4.5. Robustness against the Number of Hydrophones. The results in Figures 9–12 plotted the RMSE as a function of the number of hydrophones. As the number of hydrophones increases, the directivity also increases and hence RMSE decreases significantly. It can be seen that the FPA produces even for fewer hydrophones than the other algorithms in both cases of 5 and 10 dB of SNR.

4.6. Robustness against Snapshots. Another parameter to be considered is the impact of snapshots on RMSE. In this simulation, the SNR at 5 dB is fixed and the number of snapshots from 5 to 200 is varied with a step size of 5. Figures 13 and 14 show that as the number of snapshots increases, the RMSE decreases towards zero. The FPA outperforms the MVDR, MUSIC, RMUSIC, and ESPRIT algorithms. The worst performance of MUSIC and MVDR is due to low SNR, which results in a distorted spatial spectrum.

4.7. Analysis of Empirical Cumulative Distribution Function of RMSE. In this section, the observations of the RMSE are

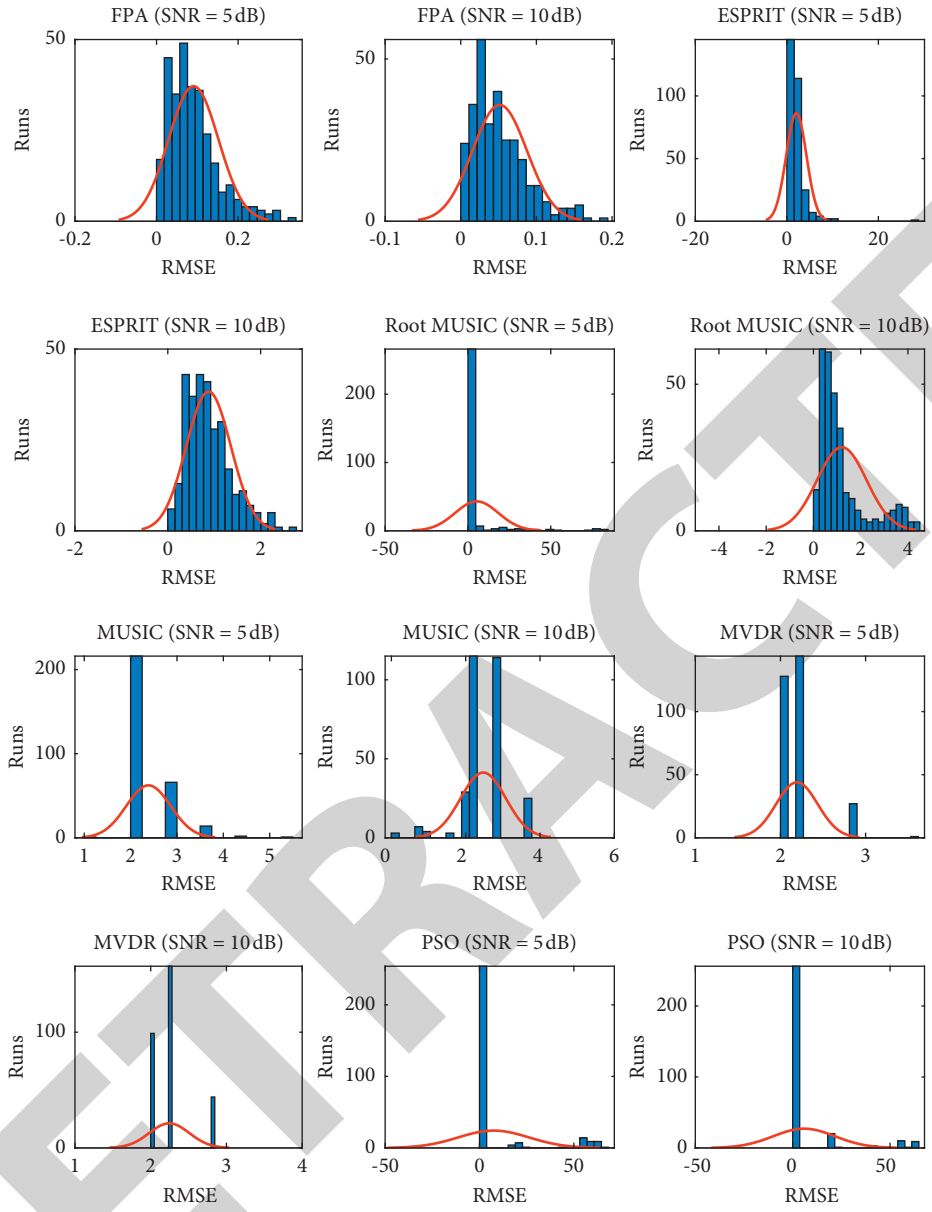

Figure 17: Histogram analysis of RMSE for two sources.

depicted in the order from least to greatest. This analysis corresponds to the survival and failure times of the algorithms over the Monte Carlo runs. It can be seen from Figures 15 and 16 that the FPA gives a significant amount of the Monte Carlo runs having the least RMSE. MVDR and MUSIC algorithms depict a colossal number of Monte Carlo trials with the most incredible value of RMSE that leads to the failure of the algorithm for DOA estimation. More specifically, the FPA and ESPRIT algorithms also give a remarkable amount of Monte Carlo trials the least RMSEs compared to PSO, MUSIC, Root MUSIC, and MVDR algorithms. Ultimately, the noteworthy performances are possessed by the FPA.

4.8. Frequency Distribution of RMSE. In this section, the histogram provides a visual interpretation of RMSE observations by showing the number of RMSE observations that fall within a specified range of RMSE values. This analysis also explains the skewness of the RMSE observations to validate the performance of the algorithms. It can be seen from Figures 17 and 18 that most of the occurrences underlie the least values of the RMSE for FPA. Furthermore, the ESPRIT algorithm gives a fair distribution of frequency of RMSE over the Monte Carlo runs compared to PSO, Root MUSIC, MUSIC, and MVDR algorithms.

4.9. Variability Analysis of the RMSE. In this section, the spread-out of the RMSE is analyzed in the five pieces of the information (minimum, first quartile, median, third quartile, and maximum) over the Monte Carlo trials. "Minimum" depicts the minimum value of the RMSE from Monte Carlo observations. In comparison, the first and

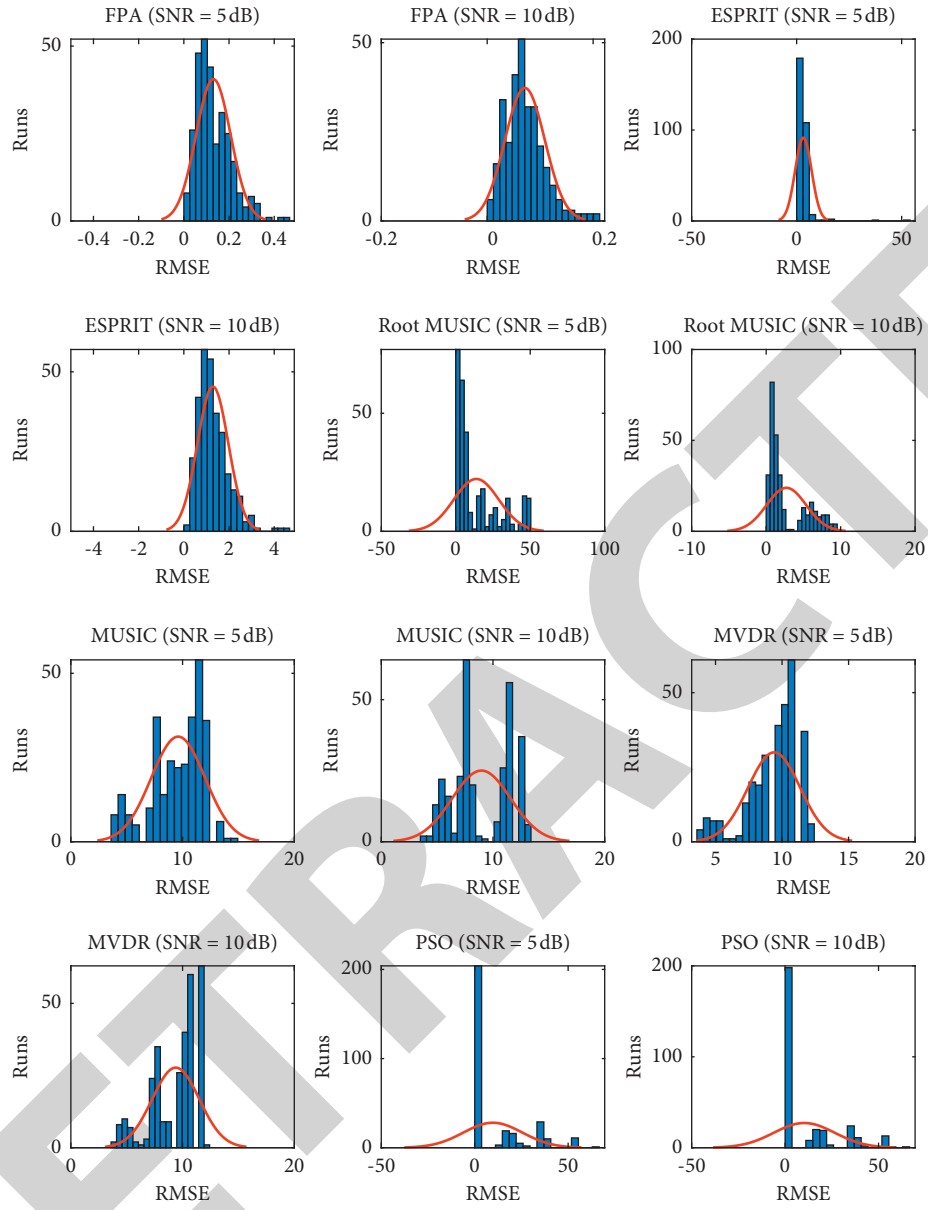

Figure 18: Histogram analysis of RMSE for three sources.

third quartiles describe 25 and 75 percent of the RMSE observations (Monte Carlo runs). This measure of the spread-out is a comprehensive description of the RMSE distribution to validate the performance of the algorithms. It can be seen from Figures 19 and 20 that FPA displays the distribution of RMSE with the least values of the RMSE, which reveals it is outperforming the other algorithms. Furthermore, the ESPRIT algorithm also gives significant performance compared to the PSO, Root MUSIC, MUSIC, and MVDR algorithms.

4.10. The Resolution Ability for Closely Spaced Targets. In this section, the simulation background is estimated for the proposed structure to check the superresolution performance. The probability of resolution is defined as

$$P_r = \text{Prob}\left[\left|\theta_e - \theta_a\right| \leq \frac{\triangle\theta}{2}\right], \tag{21}$$

where $\triangle\theta = |\theta_1 - \theta_2|$. The resolution ability of both closely spaced sources is shown in Figures 21–24. The performance is analyzed based on different DOA positions. It can be seen that the FPA outperforms the others but the PSO performs significantly too for closely spaced sources. Simulation is carried out by fixing the first source and moving the second source from 35 to 34 degrees. The resolution ability is analyzed for each separation for both sources independently.

4.11. Computational Complexity Analysis. In this, the computation loading performance is analyzed using MUSIC, MVDR, and RMUSIC algorithms, which are highly

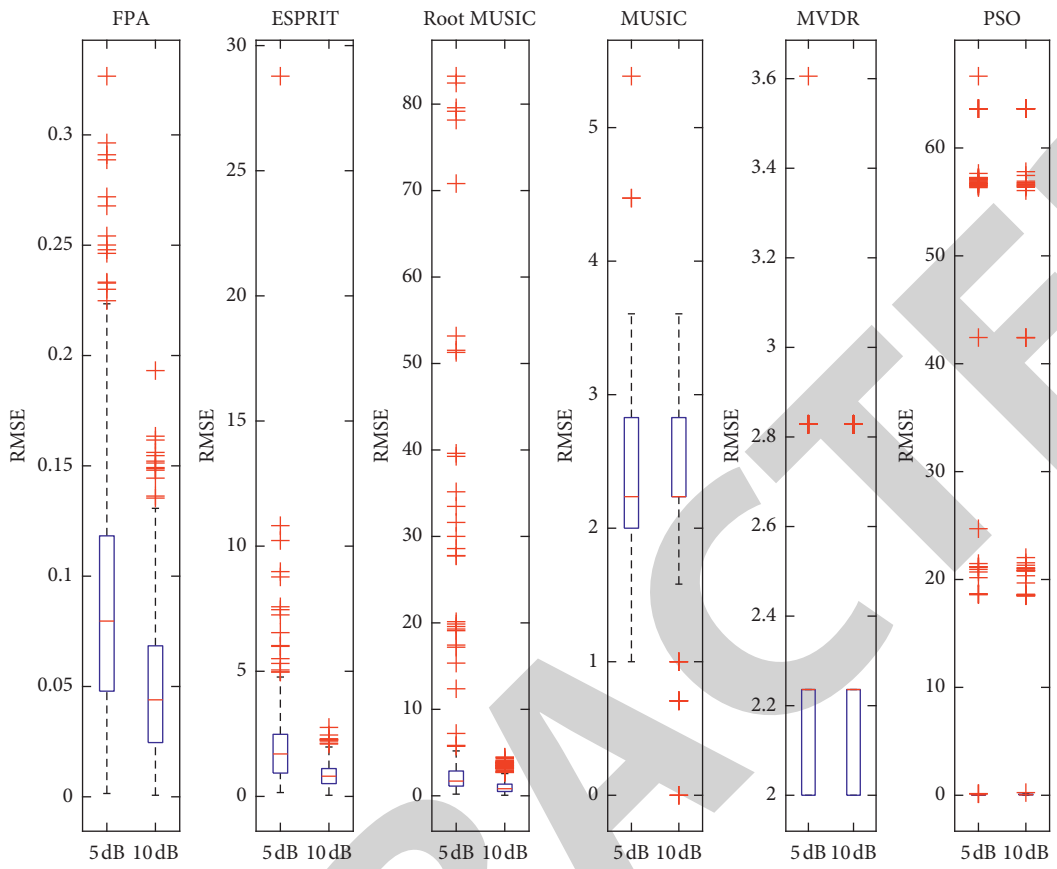

Figure 19: Variability analysis for two sources.

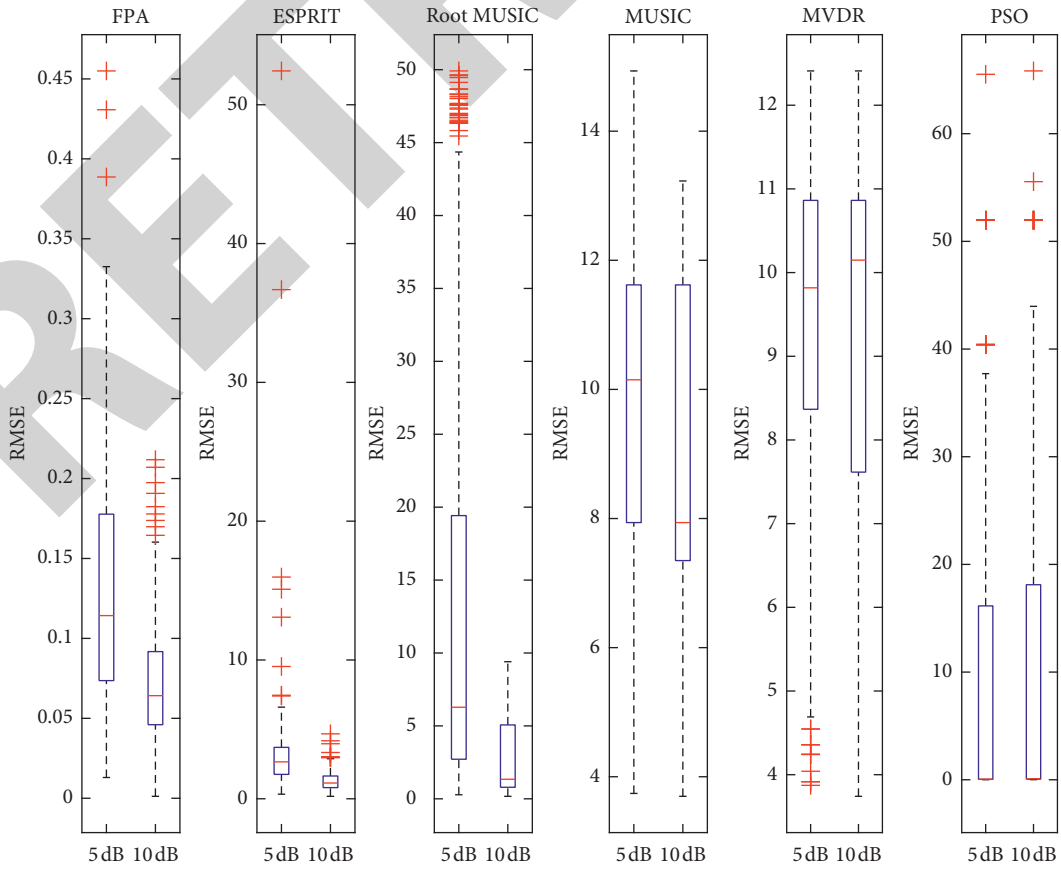

Figure 20: Variability analysis for three sources.

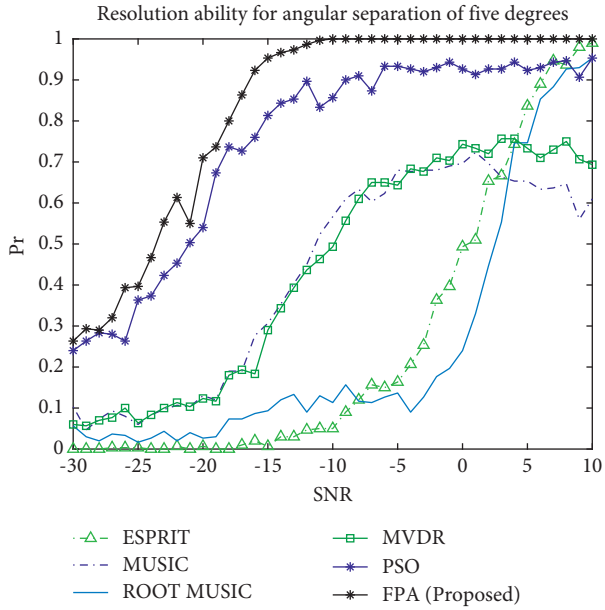

Figure 21: Probability of resolution for the source at 30 degrees.

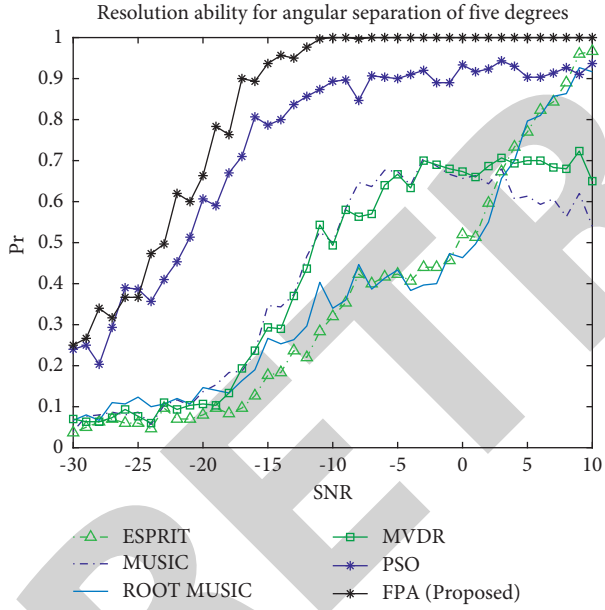

Figure 22: Probability of resolution for the source at 35 degrees.

computational practical algorithms due to their spectral search approach to estimate the DOA. Moreover, the ESPRIT algorithm neither includes the extrema search optimization nor the spectral search approach; hence, it results in better computational complexity than the other algorithms as mentioned in Table 4. The FPA also outperforms the MUSIC, MVDR, and RMUSIC algorithm but is not better than the ESPRIT algorithm due to its extrema searching approach to optimize the cost function. The extrema searching approach of FPA and PSO to optimize the cost function increases the computational complexity that sometimes restrain the application of swarming intelligent algorithms.

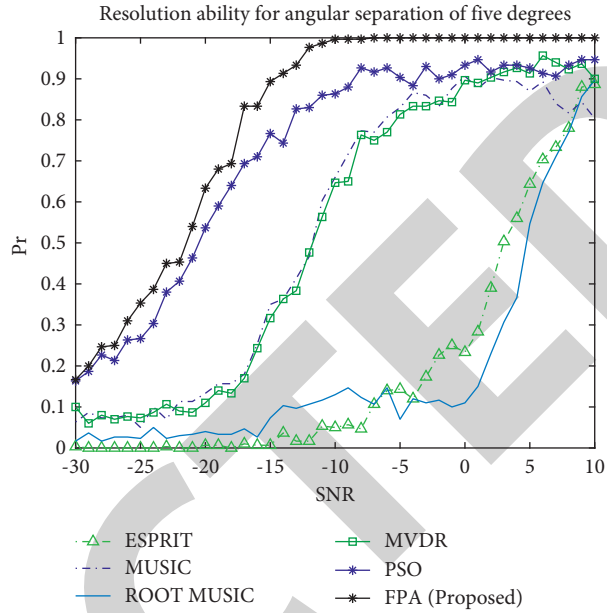

Figure 23: Probability of resolution for the source at 30 degrees.

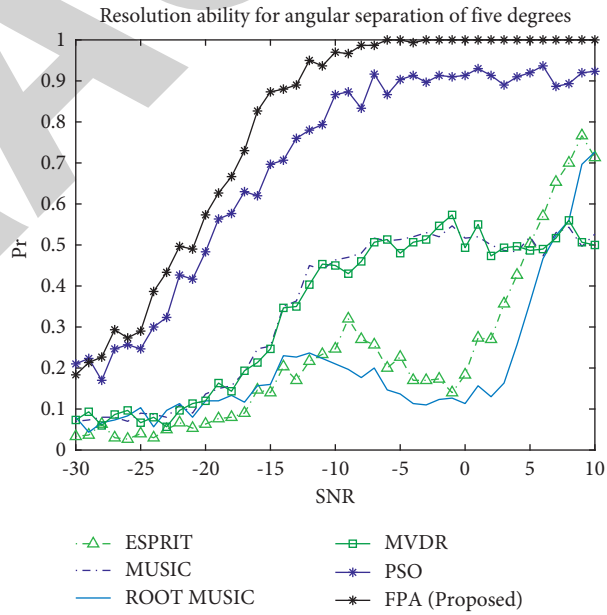

Figure 24: Probability of resolution for the source at 34 degrees.

Table 4: Computational loading analysis.

Algorithm	Complexity
MVDR	$W^2(K+6)+W+4*D*P$
MUSIC	$5/3W^3+W^2(K+1+D+W)+4*D*P$
RMUSIC	$11/3W^3+W^2(K+D-1)+2(W-1)$
ESPRIT	$W^2(K+2*W+1)+D(D+1)$
PSO	$K*T*N*W*D$
FPA	$D*T*K*N*W(1-p_s)$

5. Conclusion

The simulation results demonstrate that the FPA outperforms the conventional beamforming and conventional

subspace-based algorithms in most situations. The performance improvement is more significant when multiple signals are incident at closely spaced angles at a low signal-to-noise ratio and when a small number of snapshots are used to estimate direction of arrival (DOA). Statistical analysis of the RMSE in Monte Carlo trials, that is, ECDF of RMSE, variability analysis of RMSE, frequency distribution of RMSE, and the probability of resolution, witnesses the strength of FPA in the challenging environment of low SNR using less number of snapshots. In the future, the estimation of 2D-DOA of underwater multitargets using 2D arrays should be investigated with modern heuristic algorithms to achieve high accuracy and resolution. Moreover, the proposed flower pollination heuristics look promising to deal with the optimization problems in diversified fields.

Data Availability

No data were used to support this study.

Conflicts of Interest

The authors declare no conflicts of interest.

Acknowledgments

This work was supported in part by the Beijing Natural Science Foundation (No. 4212015), Natural Science Foundation of China (No. 61801008), China Ministry of Education-China Mobile Scientific Research Foundation (No. MCM20200102), China Postdoctoral Science Foundation (No. 2020M670074), Beijing Municipal Commission of Education Foundation (No. KM201910005025), and China National Key Research and Development Program (No. 2018YFB0803600).The authors express their gratitude to Princess Nourah bint Abdulrahman University Researchers Supporting Project (Grant no. PNURSP2022R60), Princess Nourah bint Abdulrahman University, Riyadh, Saudi Arabia.

References

[1] K. Hameed, S. Tu, N. Ahmed et al., "DOA estimation in low SNR environment through coprime antenna arrays: an innovative approach by applying flower pollination algorithm," *Applied Sciences*, vol. 11, 2021.

[2] H. Jing, H. Wang, Z. Liu, and X. Shen, "DOA estimation for underwater target by active detection on virtual time reversal using a uniform linear array," *Sensors*, vol. 18, 2018.

[3] N. Ahmed, H. Wang, M. A. Z. Raja et al., "Performance analysis of efficient computing techniques for direction of arrival estimation of underwater multi targets," *IEEE Access*, vol. 9, 2021.

[4] A. Mushtaq and G. Mahendru, "A proposed DOA estimation technique based on wavelet packet decomposition for fading channel in MIMO systems," in *Proceedings of the 6th International Conference on Signal Processing and Integrated Networks (SPIN)*, pp. 278–281, Noida, India, March 2019.

[5] Y.-F. Liang, P.-F. Jiang, J.-N. Xu, W. An, and M. Wu, "Initial alignment of compass based on genetic algorithm-particle swarm optimization," *Defence Technology*, vol. 16, no. 1, pp. 257–262, 2020.

[6] P. Wang, Y. Kong, X. He, M. Zhang, and X. Tan, "An improved squirrel search algorithm for maximum likelihood DOA estimation and application for MEMS vector hydrophone array," *IEEE Access*, vol. 7, Article ID 118343A, 2019.

[7] Y. Chen, F. Wang, J. Wan, and K. Xu, "DOA estimation for long-distance underwater acoustic sources based on signal self-nulling," in *Proceedings of the IEEE 2nd Advanced Information Technology, Electronic and Automation Control Conference (IAEAC)*, pp. 563–567, Chongqing, China, March 2017.

[8] Y. Sato, N. Kikuma, and K. Sakakibara, "Improvement of estimation accuracy by using multiple guiding sensors in DOA estimation of radio waves with VESPA algorithm," in *Proceedings of the International Symposium on Antennas and Propagation (ISAP)*, pp. 1-2, Busan, Korea (South), October 2018.

[9] X. Zhao, Y. Yang, and K.-S. Chen, "Direction-of-Arrival estimation over sea surface from radar scattering based on convolutional neural network," *Remote Sensing*, vol. 13, no. 14, 2021.

[10] Z. Zheng, W. Q. Wang, H. P. Meng, H. C. So, and H. B. Zhang, "Efficient beamspace-based algorithm for two-dimensional DOA estimation of incoherently distributed sources in massive MIMO systems," *IEEE Transactions on Vehicular Technology*, vol. 67, no. 12, Article ID 11776, 2018.

[11] A. Dixit, J. Sathyamurthy, S. Rao, S. Gurugopinath, and G. Thiagarajan, "Detection and localization of targets using millimeter wave radars: an experimental study," in *Proceedings of the IEEE International Conference on Electronics, Computing and Communication Technologies (CONECCT)*, pp. 1–6, Bangalore, India, July, 2021.

[12] V. V. Chudnikov, B. I. Shakhtarin, A. V. Bychkov, and S. M. Kazaryan, "Doa estimation in radar sensors with colocated antennas," in *Proceedings of the Systems of Signal Synchronization Generating and Processing in Telecommunications (SYNCHROINFO)*, Svetlogorsk, Russia, July 2020.

[13] X. Chen, Y. Li, Y. Li, and J. Yu, "PHD and CPHD algorithms based on a novel detection probability applied in an active sonar tracking system," *Applied Sciences*, vol. 8, no. 1, 2017.

[14] Y. Li, X. Gao, and L. Wang, "Reverse dispersion entropy: a new complexity measure for sensor signal," *Sensors*, vol. 19, no. 23, 2019.

[15] Y. Li, B. Geng, and S. Jiao, "Refined composite multi-scale reverse weighted permutation entropy and its applications in ship-radiated noise," *Entropy*, vol. 23, no. 4, 2021.

[16] S. Jeong, Y. Won, and D. Shin, "Fast doa estimation method based on music algorithm combined Newton method for fmcw radar," in *Proceedings of the IEEE MTT-S International Conference on Microwaves for Intelligent Mobility (ICMIM)*, pp. 1–5, Detroit, MI, USA, April 2019.

[17] S. Cho, H. Song, K.-J. You, and H.-C. Shin, "A new direction of arrival estimation method using automotive radar sensor arrays," *International Journal of Distributed Sensor Networks*, vol. 13, no. 6, Article ID 155014771771362, 2017.

[18] E. Schubert, F. Meinl, M. Kunert, and W. Menzel, "High resolution automotive radar measurements of vulnerable road users - pedestrians cyclists," in *Proceedings of the IEEE MTT-S International Conference on Microwaves for Intelligent Mobility (ICMIM)*, pp. 1–4, Heidelberg, Germany, April 2015.

[19] S.-H. Jeong, Y.-S. Won, and D. Shin, "Fast DOA estimation method based on MUSIC algorithm combined Newton method for FMCW radar," in *Proceedings of the IEEE MTT-S*

International Conference on Microwaves for Intelligent Mobility (ICMIM), pp. 1–5, Detroit, MI, USA, April 2019.

[20] Y. Wang, X. Yang, J. Xie, L. Wang, and B. W.-H. Ng, "Sparsity-inducing DOA estimation of coherent signals under the coexistence of mutual coupling," *Emerging Trends, Issues and Challenges for Array Signal Processing and Its Applications in Smart City*, vol. 7, 2020.

[21] M. Wu and C. Hao, "Super-resolution TOA and AOA estimation for OFDM radar systems based on compressed sensing," *IEEE Transactions on Aerospace and Electronic Systems*, vol. 1, 2022.

[22] K. Hameed, W. Khan, Y. S. Abdalla et al., "Far-field DOA estimation of uncorrelated RADAR signals through coprime arrays in low SNR regime by implementing Cuckoo search algorithm," *Electronics*, vol. 11, no. 4, 2022.

[23] P. Singh and N. Mittal, "An efficient localization approach to locate sensor nodes in 3D wireless sensor networks using adaptive flower pollination algorithm," *Wireless Networks*, vol. 27, no. 3, pp. 1999–2014, 2021.

[24] X. Zhang, L. Xu, L. Xu, and D. Xu, "Direction of departure (DOD) and direction of arrival (DOA) estimation in MIMO radar with reduced dimension MUSIC," *IEEE Communications Letters*, vol. 14, no. 12, pp. 1161–1163, 2010.

[25] S. Pazos, M. Hurtado, and C. Muravchik, "DOA estimation using random linear arrays via compressive sensing," *IEEE Latin America Transactions*, vol. 12, no. 5, pp. 859–863, 2014.

[26] J. Li, Q.-H. Lin, C.-Y. Kang, K. Wang, and X.-T. Yang, "DOA estimation for underwater wideband weak targets based on coherent signal subspace and compressed sensing," *Sensors*, vol. 18, no. 3, 2018.

[27] A. Miller, B. Miller, and G. Miller, "On AUV control with the aid of position estimation algorithms based on acoustic seabed sensing and DOA measurements," *Sensors*, vol. 19, no. 24, 2019.

[28] A. A. A. El-Banna, K. Wu, and B. M. ElHalawany, "Opportunistic cooperative transmission for underwater communication based on the water's Key physical variables," *IEEE Sensors Journal*, vol. 20, no. 5, pp. 2792–2802, 2020.

[29] X. Pan, B. Song, C. Liu, and H. Zhang, "Music detecting and recording system based on support vector machine," in *Proceedings of the International Conference on Communications, Information System and Computer Engineering (CISCE)*, pp. 244–248, Haikou, China, July 2019.

[30] A. Sharma and S. Mathur, "Comparative analysis of ML-PSO DOA estimation with conventional techniques in varied multipath channel environment," *Wireless Personal Communications*, vol. 100, no. 3, pp. 803–817, 2018.

[31] H. Wang, Y. Li, and J. Qian, "Self-adaptive resource allocation in underwater acoustic interference channel: a reinforcement learning approach," *IEEE Internet of Things Journal*, vol. 7, no. 4, pp. 2816–2827, 2020.

[32] X. Li, Y. Zhou, L. Yan, H. Zhao, X. Yan, and X. Luo, "Optimal node selection for hybrid attack in underwater acoustic sensor networks: a virtual expert-guided bandit algorithm," *IEEE Sensors Journal*, vol. 20, no. 3, pp. 1679–1687, 2020.

[33] Y. Zhang, G. Hu, M. Zhu et al., "DOA estimation based on average processing of redundant virtual array elements for coprime MIMO RADAR," *J. Phys. Conf. Ser*, vol. 1894, no. 1, Article ID 012092, 2021.

[34] S. Saha, D. Chatterjee, and B. Sarkar, "The ramification of dynamic investment on the promotion and preservation technology for inventory management through a modified flower pollination algorithm," *Journal of Retailing and Consumer Services*, vol. 58, Article ID 102326, 2021.

[35] P. E. Mergos and X. S. Yang, "Flower pollination algorithm parameters tuning," *Soft Computing*, vol. 25, no. 22, Article ID 14429, 2021.

[36] J.-S. Pan, J. Zhuang, H. Luo, and S.-C. Chu, "Multi-group flower pollination algorithm based on novel communication strategies," *Journal of Internet Technology*, vol. 22, no. 2, pp. 257–269, 2021.

[37] S. Lalljith, I. Fleming, U. Pillay, K. Naicker, Z. J. Naidoo, and A. K. Saha, "Applications of flower pollination algorithm in electrical power systems: a review," *IEEE Access*, vol. 10, pp. 8924–8947, 2022.